

Food & Function

Linking the chemistry and physics of food with health and nutrition

Accepted Manuscript

This article can be cited before page numbers have been issued, to do this please use: X. Li, E. Capuano, C. de Korte and P. Smeets, *Food Funct.*, 2026, DOI: 10.1039/D5FO04784F.



This is an Accepted Manuscript, which has been through the Royal Society of Chemistry peer review process and has been accepted for publication.

Accepted Manuscripts are published online shortly after acceptance, before technical editing, formatting and proof reading. Using this free service, authors can make their results available to the community, in citable form, before we publish the edited article. We will replace this Accepted Manuscript with the edited and formatted Advance Article as soon as it is available.

You can find more information about Accepted Manuscripts in the [Information for Authors](#).

Please note that technical editing may introduce minor changes to the text and/or graphics, which may alter content. The journal's standard [Terms & Conditions](#) and the [Ethical guidelines](#) still apply. In no event shall the Royal Society of Chemistry be held responsible for any errors or omissions in this Accepted Manuscript or any consequences arising from the use of any information it contains.

1 **Monitoring *in vitro* gastric bolus digestion with** 2 **ultrasound**

3 **Authorship**

4 Xinhang Li^{a,b}, Edoardo Capuano^b, Chris L. de Korte^c, Paul A.M. Smeets^{a*}

5 ^a Division of Human Nutrition & Health, Wageningen University & Research, Wageningen, The
6 Netherlands

7 ^b Food Quality and Design Group, Wageningen University, Wageningen, The Netherlands

8 ^c Medical UltraSound Imaging Center (MUSIC), Department of Radiology and Nuclear Medicine,
9 Radboud University Medical Center, Nijmegen, The Netherlands

10 Affiliation address: Stippeneng 4, 6708 WE, Wageningen, The Netherlands.

11 *Corresponding author. E-mail address: paul.smeets@wur.nl

13 **Abstract**

14 Monitoring food degradation during gastric digestion is essential to understand how
15 food properties impact nutrient absorption. Imaging techniques like ultrasound can
16 be used to validate *in vitro* results *in vivo*.

17 The aim was to assess the use of ultrasound (US) for monitoring changes in food
18 bolus properties during *in vitro* gastric digestion with a newly designed model system.



19 Artificial bread boli (n=9) treated with amylase, pepsin or no enzyme underwent 90
20 minutes of static digestion (INFOGEST), during which US images were recorded.
21 Bolus area and the number of pixels and Haralick image texture features were
22 calculated. Average grey values were calculated at increasing distance from the bolus
23 edge.

24 The echogenic bolus area on ultrasound images increased over 90 min. From 10-60
25 min, amylase-treated boli were larger than pepsin-treated (ratios 2.00-2.40) and no
26 enzyme boli (ratios 1.89-2.23). Regarding image texture, these boli had higher
27 homogeneity and lower contrast than pepsin-treated boli. From 30 min onward, the
28 bolus area of amylase-treated boli had 1.19-1.30 times higher homogeneity, and 2.5-
29 4% lower *entropy*. From 10 min, the slope of the mean grey value curves for
30 amylase-treated boli remained lower than for the other treatments. In the amylase-
31 treated boli, an increase in homogeneity ($\rho=0.8$) and decreases in entropy ($\rho=-$
32 0.82) and slope ($\rho=-0.85$) corresponded with increasing starch digestibility.

33 These findings show the capacity of US imaging for quantifying bolus degradation *in*
34 *vitro*. Future work should explore this novel application of US imaging in dynamic *in*
35 *vitro* models and *in vivo*.

36 **Keywords**

37 *In vitro* gastric digestion; Bolus degradation; Ultrasonography; Image texture
38 features



39 **1 Introduction**

40 Food digestion is a complex combination of physiological, mechanical and biochemical
41 processes that ultimately leads to the absorption of nutrients. These dynamic and
42 individual-specific processes make experimental studies on human digestion
43 particularly challenging. In addition, due to ethical, practical, and technical limitations,
44 direct studies of *in vivo* human digestion can be difficult to conduct.¹

45 Therefore, many *in vitro* digestion models have been developed, mimicking one or
46 more digestion phases.² These can be classified as static or dynamic models,
47 depending on their capacity to reproduce the dynamic physiological aspects of
48 digestion (e.g., gradual acidification or gastric emptying of the stomach). Static *in*
49 *vitro* models, such as the INFOGEST method,³ are widely used for assessing the
50 digestibility of various food components. While they simplify digestive physiology and
51 cannot mimic the complex dynamics of the digestive system, their straightforward
52 design is effective for evaluating the impact of key factors such as pH and enzyme
53 activity, making them quite suitable for mechanistic studies.^{3,4} *In vitro* models
54 provide controlled conditions and allow easy sampling. However, validating *in vitro*
55 results against *in vivo* human digestion is challenging. Although the level of nutrient
56 absorption can be analyzed by physiological indicators such as blood measurements,
57 more direct and non-invasive techniques are needed to observe and characterize the
58 preceding digestion mechanisms *in vivo*.

59 Validating *in vitro* findings *in vivo* may be achieved with imaging techniques such as
60 magnetic resonance imaging (MRI), which can be used to connect *in vitro* and *in vivo*
61 digestion models, because they can be used in both experimental settings.⁵ Although



62 MRI has emerged as a valuable tool in investigating gastrointestinal digestion, it is
63 relatively expensive and requires participants to be positioned in the scanner tube,
64 usually in a supine position. Another potential imaging technique is ultrasound (US)
65 imaging. This technique is more affordable, widely available, and US machines are
66 portable. US uses high-frequency acoustic beams to penetrate tissues, with
67 reflections varying depending on acoustic impedance and reflector size, which is
68 influenced by tissue properties such as density.⁶ These reflections are captured by a
69 transducer and converted into images, with the brightness of images increasing
70 proportionally to the reflection strength. Ultrasound imaging is well-established for
71 various clinical applications including preoperative assessment of the nature and
72 volume of the gastric contents.⁷ In research on gastric digestion, US has mainly been
73 used to measure the rate of gastric emptying of different foods such as rye whole-
74 meal bread and white wheat bread,⁸ and viscous guar gum.⁹ A study went beyond
75 the assessment of gastric emptying and used US to monitor changes in the
76 consistency of the gastric contents which differed in protein coagulation. For the same
77 gastric antrum cross sectional area (CSA), calculated from the anteroposterior and
78 craniocaudal diameters to represent gastric volume, lower plasma amino acid level
79 was found for participants with curds compared with those without observed curds,
80 suggesting that casein curd formation in the stomach leads to slower amino acid
81 absorption, in addition to the apparent gastric volume changes.¹⁰ This suggests that
82 US could also be used to obtain quantitative measurements reflecting the properties
83 and breakdown of ingested solid foods such as the particle size and texture. However,
84 before such a novel approach could be applied *in vivo*, *in vitro* testing and validation
85 is required to be able to establish US-based markers of digestion-related changes in



86 food properties and their interpretation. A recent *in vitro* ultrasound study used
87 through-transmission mode ultrasound with paired emitter and receiver to monitor
88 gastric fluid migration and textural softening in potato and cheese slices during *in*
89 *vitro* gastric digestion.¹¹ The effective diffusivity of the gastric fluid and the softening
90 of solid food matrix were estimated from the variation of the ultrasonic velocity.
91 Faster fluid migration and ultrasonic velocity increase were observed in potato than
92 in cheese, consistent with the greater variation in hardness. While these findings
93 indicate the potential of ultrasound for tracking digestive changes, this *in vitro* setup
94 used a non-imaging approach rather than ultrasonographic imaging.

95 The aim of this study was to develop and test an ultrasound-based experimental
96 setup for monitoring bread bolus breakdown during static *in vitro* gastric digestion,
97 and to evaluate the extent to which ultrasound image information could be used to
98 track digestion processes, including macrostructural breakdown of boli and changes
99 in water content. To our knowledge, ultrasonography has not previously been used
100 in tracking and visualizing the physical breakdown of food boli during *in vitro* gastric
101 digestion. White bread was selected as a test product because it is widely consumed,
102 and has a relatively uniform structure, which allows controlled and reproducible
103 assessment of bolus breakdown.

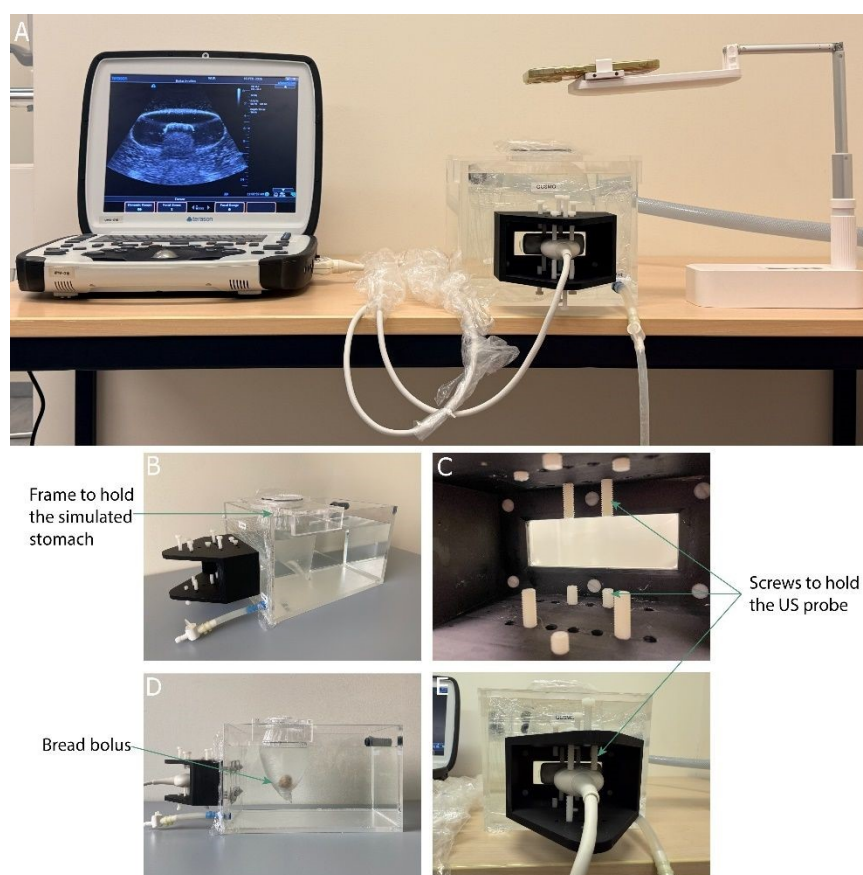
104 **2 Materials and Methods**

105 **2.1 *In vitro* set-up development**

106 We created a static *in vitro* digestion model – Gastric Ultrasound Model (GUSMO)
107 tailored to allow US imaging of the gastric content (Figure 1). It consists of a water
108 bath (30 x 22 x 18 cm) and a repositionable frame that holds a polyethylene bag,



109 simulating the stomach. The compartment can be heated and maintained at 37°C with
 110 the use of a circulating heater and a cover. We ensured compatibility with both MRI
 111 and ultrasound scanning to allow comparison of both types of measurements.
 112 Accordingly, no magnetic materials were used and a rectangular “acoustic window”
 113 sealed with thin plastic film was incorporated, allowing a seamless interface between
 114 the ultrasound probe and the water in the bath. The US probe can be secured in a
 115 stable position with screws to ensure imaging with a consistent angle.



116
 117 **Figure 1.** *In vitro* setup of the Gastric Ultrasound Model (GUSMO). (A) An overview of the setup,
 118 including the ultrasound device (left), the GUSMO model(middle), and a phone holder (right) for
 119 recording top-view images of the bolus during digestion. (B) The water bath and the repositionable
 120 frame. (C) The “acoustic window”. (D) The setup with a bread bolus in simulated stomach. (E) The US
 121 probe held by screws.



122 2.2 Preparation of bread boli

123 Commercial "Casino Wit Brood" was purchased from a local supermarket (Albert
124 Heijn®, Netherlands). It refers to a Dutch white sandwich bread, typically baked in
125 a rectangular loaf tin and pre-sliced, with a soft texture and relatively uniform crumb
126 structure. The crust was removed after which slices of bread were cut into cubes of
127 around 1 × 1 cm. Their thickness was the same as the original height of the toast,
128 around 1.3-1.5 cm.

129 Fifteen grams of bread were moistened with 5 ml liquid including water, simulated
130 saliva fluid (SSF) or gastric fluid (SGF). SSF and SGF were prepared according to the
131 INFOGEST protocol.³ Based on pilot trials, the INFOGEST 1:1 food-to-liquid ratio³
132 produced excessively hydrated boli that collapsed too rapidly for ultrasound tracking.
133 A lower ratio (15 g bread : 5 ml fluid) was therefore adopted to retain bolus integrity,
134 in line with studies suggesting lower saliva incorporation during *in vivo* mastication
135 ^{12,13}. To ensure effective contact between sample and enzymes in this static system
136 with a large SGF volume and no gastric peristalsis, enzymes were incorporated into
137 the boli during preparation rather than being added to the surrounding SGF. In
138 addition, to distinguish the individual contributions of amylase and pepsin to
139 structural changes, three different samples were produced where the 5 mL liquid was
140 either: (1) 5 ml SSF with 0.1485 g amylase, (2) 5 ml SGF with 0.0125 g pepsin or
141 (3) 5 ml Milli-Q water with no enzyme. The pepsin and amylase were diluted in
142 simulated digestive fluid. α -Amylase from porcine pancreas (A3176, 10.1 activity
143 units/mg) and pepsin from porcine gastric mucosa (P6887, 3200 activity units/mg)
144 were purchased from Sigma-Aldrich (USA). The amylase and pepsin were applied at
145 an activity of 75 U/ml and 2000 U/ml suggested by INFOGEST protocol. The total



146 enzymatic activity was calculated based on the amount of bread sample and the 5 ml
147 liquid used for bolus formation. Since enzymes were added during the bolus
148 preparation step. Enzyme activities were converted to activity (U)/ (g) nutrients. The
149 final concentration of amylase and pepsin was approximately 196 U/g carbohydrate
150 and 30307 U /g of protein.

151 After mixing with one of the above solutions, samples were manually pressed and
152 grinded 60 times using a mortar and pestle. Then the particles were collected and
153 squeezed to form a ball, after which a board was used to press gently on each side
154 to make the ball into a parallelepiped and make the surface as flat as possible.
155 Several approaches were tested to shape the bolus, including the use of molds,
156 syringes and mechanical compression using a texture analyzer. However, due to the
157 high cohesiveness and adhesiveness of hydrated bread boli, these methods were not
158 suitable, and manual shaping was adopted as a pragmatic approach. All bolus
159 preparation steps were performed by a single operator, and bolus dimensions were
160 controlled to remain within a comparable range (approximately 4-4.5 cm in length
161 and 2-2.5 cm in width and height), to minimize size variability. Representative bread
162 boli samples are shown in Figure 2.

163 **Figure 2.** Representative images of bread boli. (a) bolus with amylase (196 units/g carbohydrate), (b)
164 bolus with pepsin (30307 units/g) and (c) bolus with no enzymes.



165 2.3 Physical property measurements

166 2.3.1 Moisture content measurement of boli.

167 Before making them into the final shape ~ 0.5 g was taken of each bolus and dried
168 in a hot-air oven at 105° for 24 hours. The difference in bolus weight before and after
169 drying was used to calculate the initial (0 min) bolus moisture content percentage.

170 2.3.2 Density measurement

171 The weight of boli was measured with an analytical scale. To measure the volume,
172 the drainage method was used: boli were placed in a measurement cylinder that
173 contained a certain amount of water and then the water was pipetted out to arrive at
174 the same volume. The weight of pipetted-out water was measured to determine the
175 volume (1 g = 1 cm³). The density of the bolus (g/cm³) was calculated by dividing its
176 weight (g) by the volume of water (cm³).

177 To compare the changes in density and water content after digestion, boli with
178 amylase were placed in 800 ml SGF and incubated for 10, 30, 60, and 90 minutes.
179 After digestion, boli were picked from digestive fluid, and density and moisture
180 measurements were taken as described above. For moisture measurement, the boli
181 were dried in a hot-air oven until they were completely dry, instead of 24 hours. All
182 measurements were done in triplicate.

183 2.4 Static *in vitro* gastric digestion

184 2.4.1 Simulated *in vitro* digestion

185 For the measurement of hydrolysis products, we separated the biochemical analysis
186 from ultrasound scanning, considering the heterogeneous distribution of hydrolysates



187 inside boli during static digestion. Boli were prepared in triplicate for each trial (with
188 amylase or pepsin) and placed in beakers containing 800 ml SGF for 0, 10, 30, 60,
189 and 90 min digestion, respectively. At the end of each trial, the boli were broken
190 down in their surrounding fluid by using a food mixer for 30 s, and three 1 ml samples
191 of the supernatant were collected. A workflow was shown as Figure S1 in
192 Supplementary data.

193 To stop the starch hydrolysis, absolute ethanol was added at a 1:4 ratio, mixed for
194 10 s and centrifuged at 10000 g for 10 min. For protein hydrolysis, the pH of sample
195 was neutralized to around 7 by adding 1 M NaOH, followed by mixing for 10 s and
196 centrifuging at 10000 g for 30 min. The centrifuged samples were stored in a freezer
197 at -20°C until further analysis.

198 2.4.1.1 Percent of digested starch

199 The supernatant taken from centrifuged samples was analyzed via measurement of
200 the overall degree of hydrolysis quantified as glucose equivalent, using GOPOD
201 format D-glucose Assay kits (Neogen, USA). To begin, 0.1 ml of supernatant was
202 mixed with 0.5 ml amyloglucosidase solution in acetate buffer (0.1M, pH 4.8) to
203 convert all the products of amylase hydrolysis into glucose. The samples were then
204 incubated at 37°C for 1 hour to allow enzymatic hydrolysis, and heated to 100°C for
205 10 min to inactivate enzyme.

206 After adding 3 ml of GOPOD reagent to 0.1 ml of sample solution, 200 μ L of the
207 mixture was sampled to a microplate. The percentage of digested starch was
208 estimated by spectrophotometry ($\lambda=510$ nm). The results were converted into starch
209 equivalent concentrations using a conversion factor of $\times 0.9$. The degree of starch



210 hydrolysis at each time points was corrected using an initial blank prepared from
211 blended no enzyme boli in SGF.

212 2.4.1.2 Degree of protein hydrolysis

213 The degree of protein hydrolysis was determined by measuring the concentration of
214 released amino groups (-NH₂ groups) using the OPA (o-phthaldialdehyde) method.
215 Serine standard solutions were used to generate a calibration curve for free amino
216 acid groups. 15 mg 105.09 g/mol serine was diluted in 100 ml MilliQ water to prepare
217 a L-Serine stock solution. Eight serine solutions with concentrations of 0, 12.5, 25,
218 50, 75, 100, 150 and 200 mg/L were prepared by proportionally diluting the stock
219 solution with water. The OPA solution was prepared just before measurement. 3.81
220 g sodium tetraborate was diluted in 80 ml MilliQ water. Once the sodium tetraborate
221 was dissolved, 0.088 g dithiothreitol and 0.1 g sodium dodecyl sulphate were added.
222 0.08 g OPA was dissolved in 3 ml ethanol and was transferred to the 80-ml solution
223 mentioned above after which MilliQ water was added to make a 100-ml solution. 24
224 μ L of sample solution was mixed with 180 μ L OPA reagents in microplates. The
225 microplates were shaken in a microplate reader for 120 s and then read at $\lambda = 340$
226 nm to quantify the concentration of amino groups.

227 Bread samples of ~ 0.3 g were used for acid hydrolysis that was performed in triplicate.
228 2 ml of 6M HCl was added to the bread in heating tubes. After heating at 110°C for
229 24h, the contents were neutralized with 1M NaOH. 0.1 ml of the neutralized solution
230 was diluted 50 times with Milli Q water. The concentration of amino acids was
231 measured following the steps mentioned above. Degree of hydrolysis (DH) was
232 expressed as the percentage of free amino groups released during digestion at 0, 10,



233 30, 60 and 90 min to the total amino groups released of complete hydrolysis, after
234 correction by subtracting the initial blank, using the following formula:

$$235 \quad DH (\%) = \frac{[Amino\ groups]_{digested} - [Amino\ groups]_{initial}}{[Amino\ groups]_{acid\ hydrolyzed} - [Amino\ groups]_{initial}} \times 100$$

236 where $[Amino\ groups]_{digested}$ is the amount of free amino groups measured in the
237 supernatant from blended pepsin-treated boli in SGF at a digestion time, $[Amino$
238 $groups]_{acid\ hydrolyzed}$ is the amount after complete acid hydrolysis, and $[Amino$
239 $groups]_{initial}$ represents the amount detected in the supernatant from blended no
240 enzyme boli in SGF.

241 2.4.2 *In vitro* gastric digestion in the GUSMO

242 Boli were digested for 1.5 hours in 800 ml simulated gastric fluid. Reducing the
243 volume was not feasible due to technical constraints related to the pressure of the
244 surrounding water and imaging requirements. They were placed at the center of the
245 bottom of the plastic bag. The initial pH of the SGF was adjusted to around 3.0 using
246 1M HCL. With the circulating heater system, the temperature of the SGF was kept at
247 37 °C.

248 2.4.3 Ultrasound setting and measurements

249 US measurements were conducted with the use of a Terason uSmart 3300 ultrasound
250 scanner (Terason®, USA) with a 5C2A curved linear array probe. The imaging settings
251 used were as follows: scan depth, 15 cm; in-plane focus distance, 6 cm; dynamic
252 range/contrast, 66 dB; frequency, 2.3 MHz; resolution, 0.0279 cm/pixel. Image Map
253 F was used. The grey value distribution profile obtained from the image map
254 reference bar showed that the grey values within the relevant range represented in



255 the acquired images were approximately linear. The gain and time gain compensation
256 settings were kept constant throughout all imaging sessions.

257 US images of the gastric compartment were obtained at baseline (empty stomach
258 compartment) and after placement of each bread bolus at 0, 5, 10, 15, 20, 25, 30,
259 35, 40, 45, 50, 55, 60, 75 and 90 min.

260 2.4.4 Image analysis

261 Boli were segmented by manually tracing their outer boundaries using wand tool, and
262 the number of pixels was calculated (Figure 3B) by the software QuPath 0.5.1
263 (University of Edinburgh, UK).¹⁴ The segmentation was initiated from a seed point
264 and expanded based on pixel intensity similarity and spatial continuity. The seed
265 point was selected within visually representative regions of the bolus (typically
266 relatively homogeneous and higher-intensity areas). In regions where the boundary
267 between the hyperechoic bolus and the surrounding background showed a clear
268 intensity transition, ROI delineation could be performed consistently. In lower
269 contrast regions, where the bolus was not sufficiently distinct, the segmentation was
270 adjusted using local intensity transitions and adjacent discontinuous hypoechoic
271 background patches as cues to exclude background and image noise (examples are
272 shown as Figure S2 in Supplementary). When the segmented regions approached the
273 stomach wall (identified as a curved boundary), the brush tool was used to exclude
274 areas within ~ 15 pixels of the wall to minimize artefacts caused by echo reflections
275 at the plastic wall boundary. An example can be found in Figure 3C. In addition, a
276 size constrained cut-off method based on estimated bolus size was used as a
277 supplementary analysis. Bolus size at each digestion time point was estimated by
278 scaling from its physical size at T0, using the frame opening diameter (7 cm), and



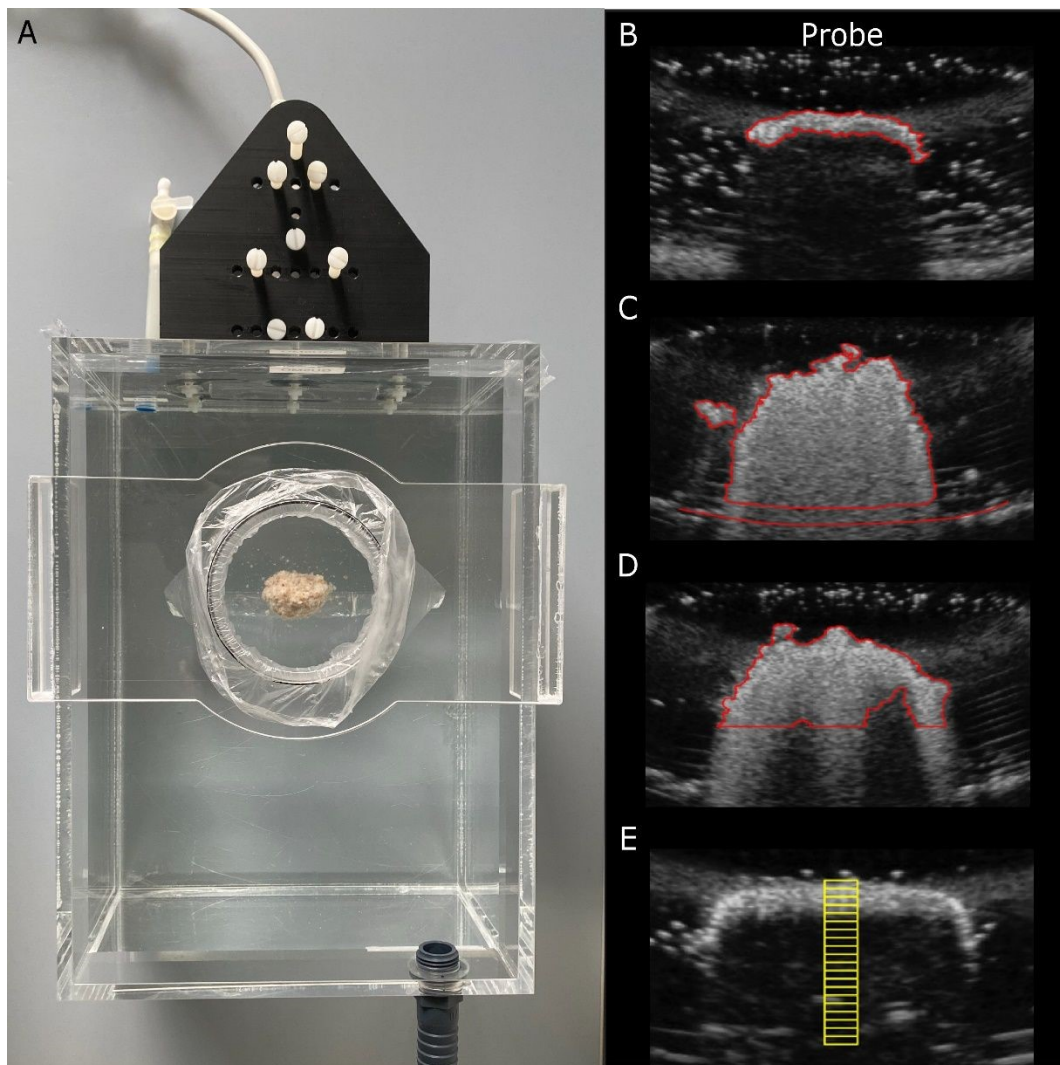
279 corresponding measurements from simultaneously captured top-view images. The
280 estimated bolus width was then used as an upper boundary to constrain the
281 segmented regions (Figure 3D). Further details and results are provided in the
282 Supplementary (Figure S3 and S4).

283 Five Haralick features including *Energy* (*Angular second moment, ASM; hereafter*
284 *referred to as "homogeneity" in this study*), *Contrast*, *Correlation*, *Inverse Difference*
285 *Moment (IDM; hereafter referred to as "local homogeneity")*, and *Entropy* were
286 calculated for the bolus pixels based on Grey Level Co-occurrence Matrix (GLCM)
287 which compares differences between neighboring pixels at 0°, 45°, 90° and 135°
288 orientations.¹⁵ These five features represent complementary aspects of image texture
289 and constitute a widely adopted subset of the 14 Haralick features.¹⁶⁻¹⁹ *Energy*
290 (*Homogeneity*) measures the uniformity or orderliness of the texture. *IDM* (*local*
291 *homogeneity*) measures the similarity of grey values. *Contrast* measures local
292 fluctuations and variations among pixels. *Correlation* reflects the linear dependency
293 of grey levels on those of its neighbors' intensity. *Entropy* represents the randomness
294 and complexity of greyscale distribution.

295 20 regions of interest (ROIs), each containing 100 pixels (20 by 5 pixels), were
296 manually placed at increasing distance from the edge of the bolus (Figure 3E),
297 gradually extending further away from the probe, which was locates at the top center
298 of the ultrasound images. The mean grey value and standard deviation were
299 calculated for each ROI using the software FIJI 2.16.0/1.54p (Fiji Is Just ImageJ,
300 National Institutes of Health, US).²⁰ Subsequently, for each ultrasound image, the
301 mean ROI grey value was plotted against the distance to the edge of the bolus. An
302 example is shown in Figure 4. To quantify the grey value trend, the slope of each line



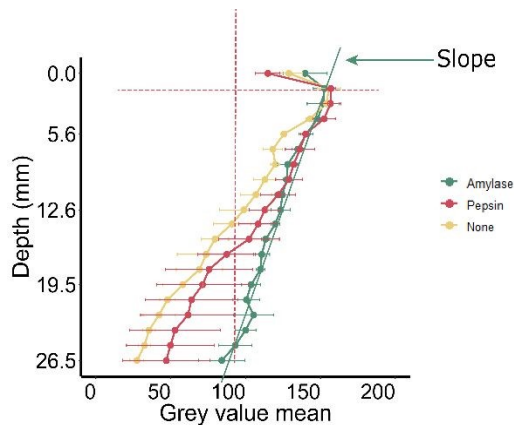
303 was calculated using the maximum point and the first point at which the mean grey
304 value dropped below 100 (Figure 4). The threshold of 100 was selected to minimize
305 the influence of slight fluctuation of grey value in some images, especially in deeper



306 ROIs, which may lead to inaccurate slope calculations.

307 **Figure 3.** Illustration of probe situation and ultrasound images. (A) Top view of a bolus in the gastric
308 compartment. (B) Bolus segmentation. The position of the probe is the same as that shown in (A). The
309 red trace indicates the outer area of the bolus. (C) Bolus segmentation and drawn stomach wall. The
310 area between the lower edge of the segmented bolus and the stomach compartment wall (lower red
311 line), within ~ 15 pixels of the wall (lower red line), was removed. (D) Constrained bolus area according
312 to estimated bolus width during digestion. (E) The yellow rectangles on the image represent 20 regions
313 of interest (ROIs), each containing 100 pixels. They are arranged at increasing depth from the edge of
314 the bolus from closest to the probe to its core (farthest from the probe).





315

316 **Figure 4.** Illustration of how the slope of the mean grey value curve was determined. The intersections
 317 of the red dashed lines with the grey value curve represent the peak point and the first point where the
 318 mean grey value dropped below 100. The slope of the green line connecting these points was calculated.

319 2.5 Statistical analysis

320 All statistical analyses were performed in R 4.5.0. Normality of the data was assessed
 321 with quantile-quantile (Q-Q) plots of the residuals of dependent variables. The plots
 322 showed substantial deviations from normality, particularly with right tails, which
 323 violated the assumptions of linear models. Using a General Linear Mixed Model (GLMM)
 324 with a Gamma distribution and a log transformation of the dependent variables led
 325 to improvement in the distribution and outcomes. Model residuals were assessed
 326 using the *DHARMA* package to verify assumptions of homoscedasticity and model fit.

327 The model included main effects of enzyme treatments (Amylase, Pepsin, No
 328 enzyme), digestion timepoints (0, 10, 30, 60, 90 min), and treatments*time
 329 interactions, and sample as a random effect to account for repeated measures within
 330 samples. The dependent variations included slopes of mean grey value, size of bright
 331 areas and GLCM image features. This model was fitted using the *glmmTMB* package
 332 in R, and Type II Wald chi-square test was used to test the fixed effects using Anova
 333 function in *car* package. P values for the main effects and interactions were adjusted



334 using Benjamini-Hochberg false discovery rate (FDR) correction used to control false
335 positives. Statistical significance was set at $p < 0.05$. *Post hoc* pairwise comparisons
336 were performed using estimated marginal means with Tukey test, and were only
337 reported when the FDR-adjusted p-values of interactions indicated significance. All
338 comparisons were based on differences between estimated marginal means, which
339 represent the log-scale difference between conditions. Coefficients in log-scale were
340 transformed to the original scale by taking the exponential of the estimates using the
341 *exp* function. The back-transformed data were shown as estimated ratios with 95%
342 confidence interval (CI) and p value (ratio, 95% CI, p). Estimated ratios represent
343 the ratio of means between any two factor levels, such as the estimated ratio of mean
344 homogeneity between amylase-treated and pepsin-treated boli. One-way ANOVA was
345 used to analyze the changes in bolus moisture over time. Spearman correlation
346 coefficients were calculated for digestibility of starch and protein, and the
347 homogeneity, entropy and grey value curve slopes.

348 **3 Results and Discussion**

349 **3.1 Monitoring structural breakdown by ultrasound images**

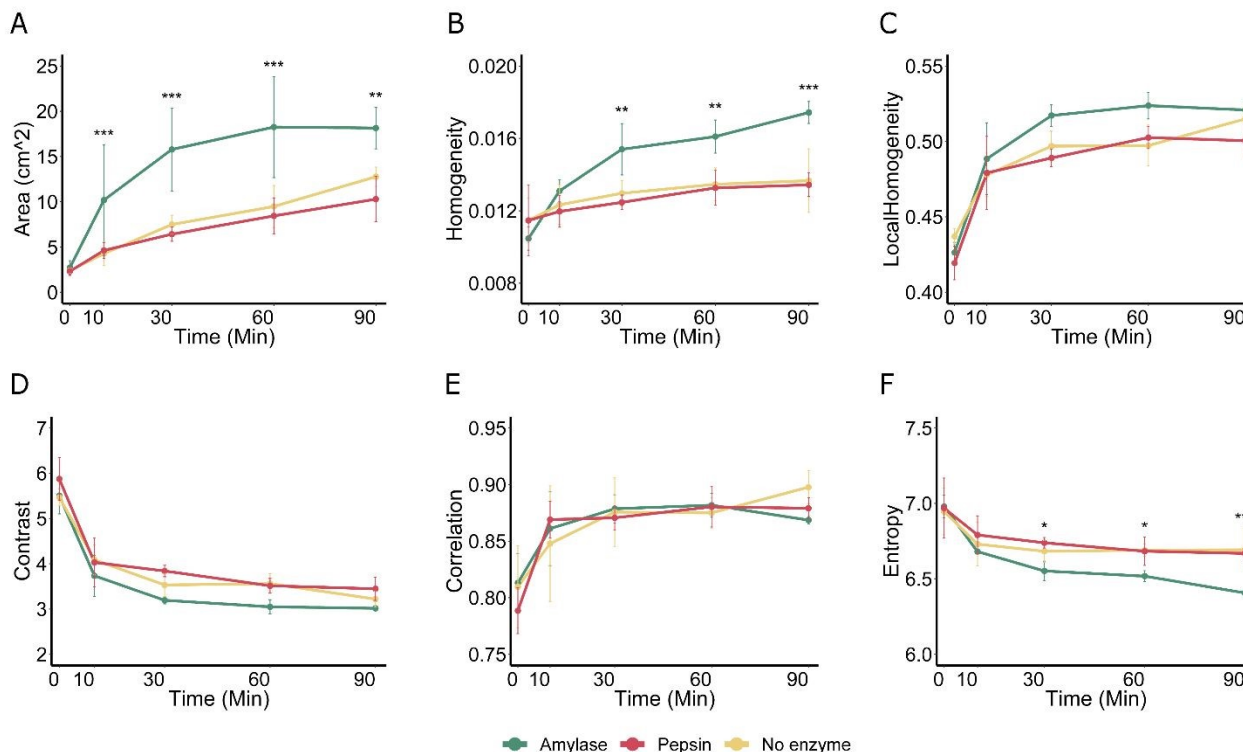
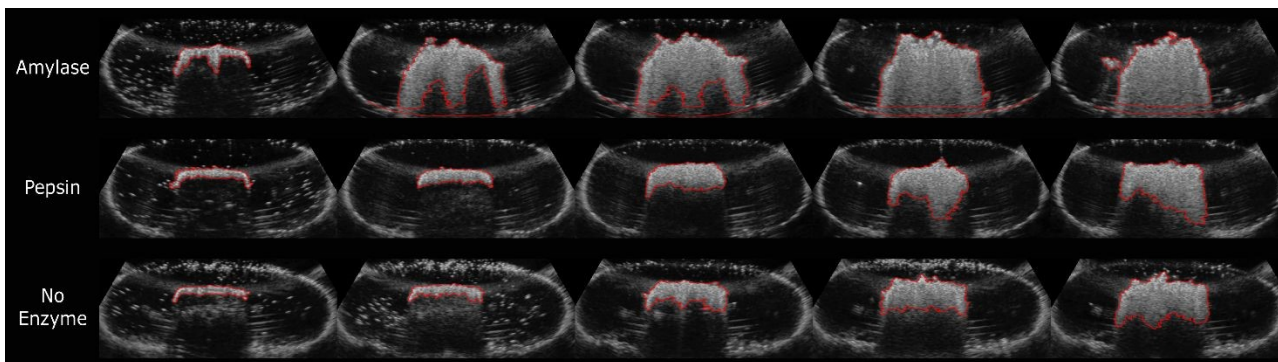
350 **3.1.1 Bolus size**

351 Figure 5 shows examples of segmented bolus areas (top panel) and the results of the
352 bolus area and image texture feature analysis. Consistent with changes visible in the
353 ultrasound images, there was a strong main effect of time on the size of boli ($\chi^2=845$,
354 $p_{\text{FDR}} < 0.0001$). The bolus area increased progressively from 0 to 90 minutes across
355 all experiments. This reflects swelling of the boli during digestion. The main effect of
356 enzyme treatment ($\chi^2=22.6$, $p_{\text{FDR}} < 0.0001$) and the interaction of time and treatment



357 were found ($\chi^2=36.3$, $p_{\text{FDR}}<0.0001$). Comparison of the enzyme treatments at each
358 time point showed that as expected there was no difference in bolus size between
359 the treatments at 0 min. From $t=10$ to $t=60$ min, the bolus size of amylase-treated
360 boli was larger than that of pepsin-treated boli and of boli with no enzyme ($p<0.001$)
361 (Table 1). At $t=90$ min, it was larger than pepsin-treated boli ($p<0.01$) but not
362 significantly different from that of no enzyme boli ($p=0.1$). The largest difference
363 was found at 30 min, when the size of amylase-treated boli was on average 2.40
364 times ($p<0.0001$) larger than that of pepsin-treated boli. For the comparison between
365 amylase and no enzyme treatments, the greatest difference was found at 10 min,
366 with the amylase-treated boli being on average 2.23 ($p<0.0001$) times larger than
367 the no enzyme boli. There were no differences between the pepsin-treated and the
368 control boli at any time point (all $p\geq 0.38$).





369 **Figure 5.** Representative images of bolus inserted in amylase (Top row), pepsin (Middle row) and no
 370 enzyme (Bottom row) with segmentation and results (A-F) of GLCM texture analysis for the traced
 371 regions over the 90-minute digestion. A: Size of segmented bolus ROIs B: Homogeneity measures the
 372 uniformity or orderliness of the texture. Higher values indicate less texture complexity; C: Local
 373 homogeneity represents similarity of grey values. Higher values indicate a smoother image/area; D:
 374 Contrast reflects differences in greyscale intensities. Higher contrast values indicate greater differences;
 375 E: Correlation reflects the degree to which a pixel's intensity is linearly related to its neighbor's intensity;
 376 F: Entropy represents the randomness and complexity of greyscale distribution; higher entropy values
 377 indicate more complex and disordered texture. Asterisks (*) indicate significant differences for amylase-
 378 treated boli compared to pepsin-treated and no enzyme boli. * p < 0.05, ** p < 0.01, *** p < 0.001. For
 379 bolus area at t=90 and Entropy at t=30, the significance refers only to amylase versus pepsin.

380 **Table 1.** Pairwise comparisons for the treatments × time interaction on bolus size.

Treatment Comparison	Time (min)	Ratio ¹	95% CI	p
Amylase / No enzyme	0	1.11	0.74, 1.67	0.81



	10	2.23	1.49, 3.35	<0.0001
	30	2.07	1.38, 3.10	0.0001
	60	1.89	1.26, 2.83	0.0007
	90	1.42	0.95, 2.13	0.1
Amylase / Pepsin	0	1.15	0.77, 1.73	0.69
	10	2.00	1.33, 3.00	0.0002
	30	2.40	1.60, 3.60	<0.0001
	60	2.12	1.42, 3.18	<0.0001
	90	1.79	1.19, 2.68	0.002

381 ¹ Estimated ratio of marginal mean bolus size for amylase-treated boli to that of no enzyme boli or the
382 pepsin-treated boli. Ratio and 95% CI are back-transformed from GLMM contrasts on the log scale.

383 These results indicate that ultrasonography can be used to track changes in the
384 swelling of boli during *in vitro* gastric digestion. The addition of amylase promoted
385 bolus expansion and degradation, while pepsin-treated boli hardly differed from the
386 control boli with no enzyme added. As digestion progressed, we observed an increase
387 in the bolus area over time. The expansion during digestion is consistent with matrix
388 weakening caused by hydrolytic process, which improves water penetration and
389 structural softening, as previously reported in gastric digestion studies.²¹ When
390 hydrolytic effects on the matrix components are limited, structural changes and
391 associated swelling are correspondingly weakened. This interpretation is supported
392 by previous finding showing limited proteolysis of bread proteins during gastric
393 digestion.²²

394 In the present study, the boli may undergo a transition from a heterogeneous,
395 consisting of fine bread chyme, porous bread crumbs and entrapped gas pockets. As



396 digestion progressed, fluid infiltration may reduce these structural differences,
397 resulting in a more uniform structure with a more homogeneous density distribution.
398 In addition, the small air pockets within the boli induce scattering and attenuation of
399 sound waves. This is because the small air inclusions have a high attenuation
400 coefficient, preventing further penetration of the ultrasound in the bolus. This is
401 clearly illustrated at $t=0$, where the heterogeneous structure of bolus and small air
402 pockets lead to strongly reduced penetration and result in only tiny bright areas.
403 From 10 to 90 min, as gastric fluid infiltrates the boli, these air pockets will be
404 dissolved and replaced by water, which would cause a decrease in attenuation and a
405 gradual increase in penetration. This would result a larger bolus area in the
406 ultrasound images. Consequently, we used image texture features, which have been
407 shown to be useful to characterize material properties.^{23,24}

408 3.1.2 Image texture: Haralick features

409 Among all the 5 Haralick features, *homogeneity* and *entropy* showed the largest
410 difference across groups. For *homogeneity*, the GLMM results showed main effects of
411 enzyme treatment ($\chi^2=19.4$, $p_{\text{FDR}}=0.0001$) and digestion time ($\chi^2=116$,
412 $p_{\text{FDR}}<0.0001$), as well as an interaction of treatment and time ($\chi^2=36.4$,
413 $p_{\text{FDR}}<0.0001$). From 30 to 90 min, the bolus areas of amylase-treated boli had higher
414 *homogeneity* than control boli and pepsin-treated boli (Table 2). The largest
415 difference in *homogeneity* was observed at 90 min, and the *homogeneity* of amylase-
416 treated boli was on average 1.30 and 1.28 times higher than that of pepsin-treated
417 boli and no enzyme boli ($p<0.0001$ and $p<0.0001$, respectively). No difference was
418 found between no enzyme boli and those with pepsin (all $p\geq 0.77$).



419 **Table 2.** Pairwise comparisons for the treatments \times time interaction on homogeneity.

Treatment Comparison	Time (min)	Ratio ¹	95% CI	p
Amylase / No enzyme	0	0.92	0.80, 1.04	0.26
	10	1.06	0.93, 1.21	0.53
	30	1.19	1.04, 1.36	0.0068
	60	1.20	1.05, 1.37	0.0044
	90	1.28	1.12, 1.46	<0.0001
Amylase / Pepsin	0	0.92	0.80, 1.05	0.27
	10	1.10	0.96, 1.25	0.24
	30	1.24	1.08, 1.41	0.0006
	60	1.21	1.06, 1.39	0.0018
	90	1.30	1.14, 1.48	<0.0001

420 ¹Estimated ratio of marginal mean homogeneity for amylase-treated boli to that of no enzyme boli or
421 the pepsin-treated boli. Ratio and 95% CI are back-transformed from GLMM contrasts on the log scale.

422 Similarly, the GLMM results showed main effects of enzyme treatment ($\chi^2 = 16.0$,
423 $p_{\text{FDR}} = 0.0004$) and digestion time ($\chi^2 = 146$, $p_{\text{FDR}} < 0.0001$), as well as an interaction
424 of treatment and time ($\chi^2 = 20.5$, $p_{\text{FDR}} = 0.017$) for the *entropy* of the bolus areas.
425 *Entropy* in amylase-treated was 97% of that in pepsin-treated and no enzyme boli at
426 $t = 60$ min ($p = 0.031$ and $p = 0.023$). At $t = 90$ min, *entropy* of amylase-treated boli
427 was approximately 4% lower than that of pepsin-treated and no enzyme boli
428 ($p = 0.0001$ and $p < 0.0001$). In contrast, there were no differences between the pepsin
429 and no-enzyme boli (all $p \geq 0.64$).

430 For *local homogeneity* and *contrast*, a main effect of treatment was observed with
431 the bolus areas of amylase-treated boli having a higher *local homogeneity* ($\chi^2 = 17.8$,



432 $p_{\text{FDR}}=0.0002$) and lower contrast ($\chi^2=23.4$, $p_{\text{FDR}}<0.0001$), than no enzyme and
433 pepsin-treated boli. For *correlation*, there was no main effect of treatment, but an
434 effect of time ($\chi^2=143$, $p_{\text{FDR}}<0.0001$). No treatment*time interaction was found in
435 *local homogeneity*, *contrast* and *correlation* (*local homogeneity*, $p=0.09$, *contrast*,
436 $p=0.22$, *correlation*, $p=0.21$). Overall, these results demonstrate that digestion
437 progression was reflected in all 5 Haralick features. Amylase, but not pepsin induced
438 increased bolus *homogeneity*, and reduced *entropy* on ultrasound images which likely
439 reflects bolus degradation. This is consistent with previous studies on starch-rich food
440 digestion, where starch hydrolysis has been shown to contribute to food matrix
441 breakdown and a softer structure.²⁵ Such structural breakdown and mixing processes
442 are known to lead to a more homogeneous digesta. In contrast, limited proteolysis
443 in gastric phase may provide context for the relatively minor changes at macroscopic
444 level observed in starch-rich bread.²⁶

445 As *homogeneity* indicates the uniformity and smoothness within an image, and
446 *entropy* measures the disorder, randomness and complexity of pixels, these results
447 suggest that the image texture is more uniform due to enzymatic breakdown and
448 fluid infiltration. Moreover, as shown in Figure 5, the trends of *contrast*, which
449 captures the variations in intensity between a reference pixel and its neighbors, were
450 opposite to those of *homogeneity* and *correlation*. Ultrasonography with GLCM
451 analysis has widely been used in clinical diagnosis. For example, a study developing
452 a non-invasive, automatic approach for diagnosing abdominal malignant tumors,
453 including the hepatocellular carcinoma and the colo-rectal tumors, found that GLCM
454 *homogeneity* and *contrast* characterized the heterogeneity of tumoral tissue arising
455 from the coexistence of regions with necrosis, fibrosis, and active growths.²⁷



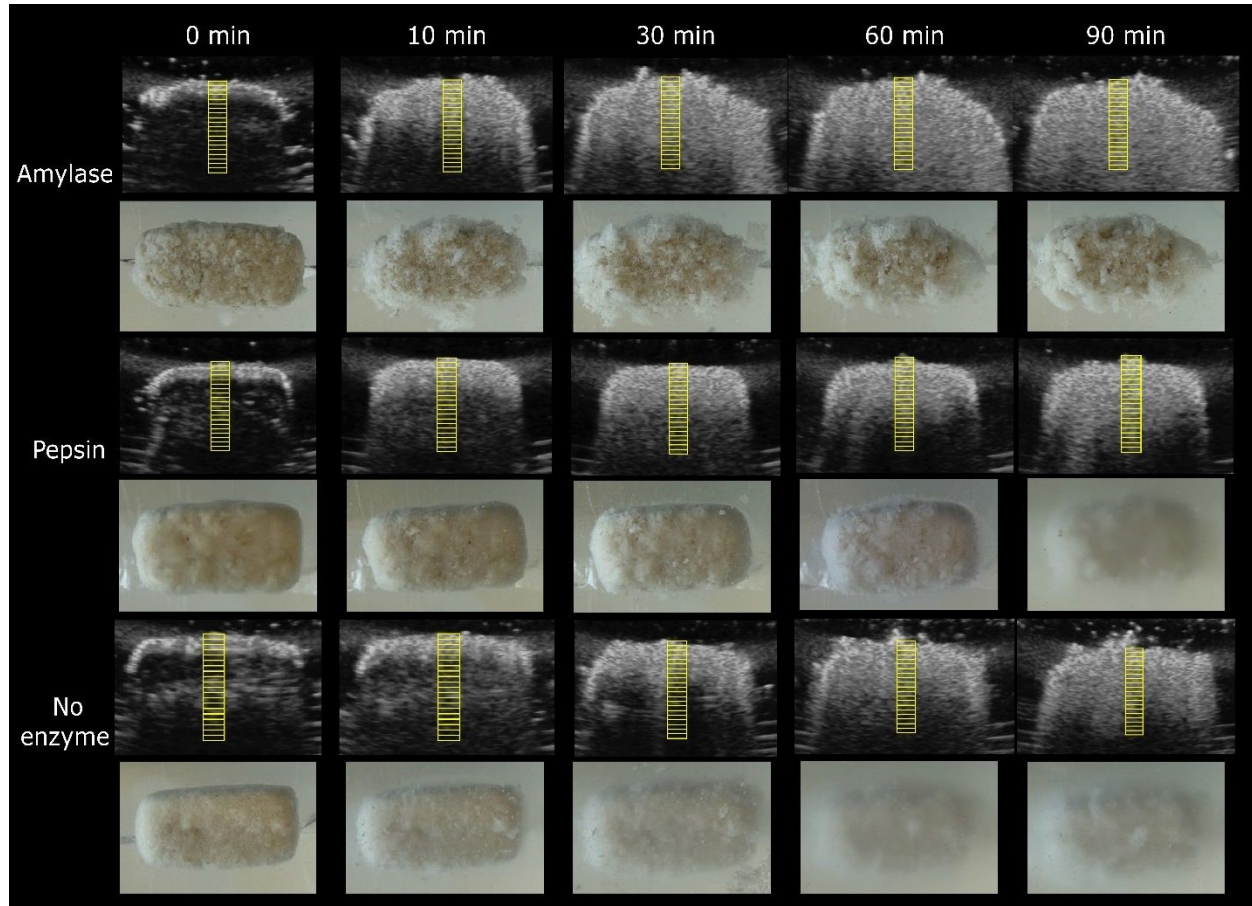
456 Quantitative image analysis showed that normal livers have higher *homogeneity* and
457 lower *contrast* than fibrotic livers, reflecting well-organized tissue architecture of
458 healthy liver tissue and the structural disorganization associated with fibrosis.²⁸ This
459 results was also consistent with an MRI study, which found that *entropy* and *contrast*
460 were good discriminative features for identifying fibrosis.²⁹ MRI studies on
461 coagulation during gastric digestion found that lower *homogeneity* and higher
462 *contrast* could indicate a higher degree of coagulum formation, and higher
463 *homogeneity* may reflect not only a more homogenous liquid, but also the presence
464 of a large and fairly homogenous coagulum.^{24,30} These findings suggest that the
465 increase in *homogeneity* and *correlation*, along with decrease *contrast* and *entropy*
466 in our study may be attributed to reduced heterogeneity of bolus during digestion.

467 3.1.3 Bolus grey value analysis

468 Figure 6 shows representative bolus pictures and corresponding ultrasound images
469 that show swelling and breakdown of the samples over the 90-minute simulated
470 gastric digestion. In all treatments, the high-echogenicity (bright) regions gradually
471 expand, regardless of enzyme addition. At time 0 the bright areas on the ultrasound
472 images are consistently small for all treatments, indicating that soundwaves have
473 only limited penetration probably caused by the presence of small air bubbles leading
474 to severe attenuation of the ultrasound signal. However, from 10 minutes onwards,
475 significant expansion of the bright bolus areas can be observed in amylase-treated
476 boli (Figure 6, top panel) compared with the other two treatments (middle and
477 bottom panels). These changes are consistent with what can be seen in the
478 photographs. Amylase-treated boli appeared more swollen with visible fragmentation
479 at the periphery, while for boli with pepsin and no enzyme, minimal changes are



480 visible over time. Overall, these ultrasound images show that ultrasonography can
481 be used to track macrostructural changes in food boli during gastric digestion.

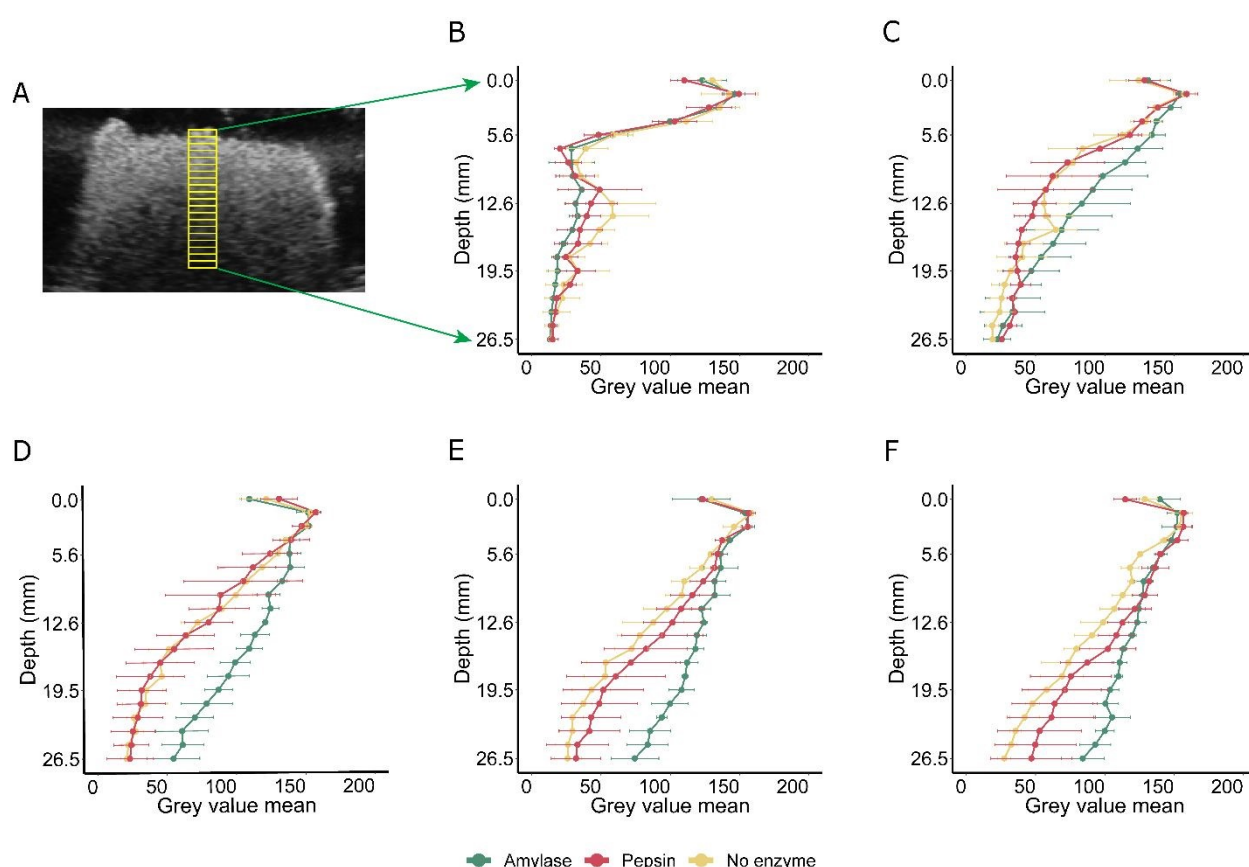


482 **Figure 6.** Representative ultrasound images and pictures of bread boli taken at different digestion time
483 points. The panels, from top to bottom, show images of bread boli containing amylase, pepsin or no
484 enzyme (control). The yellow rectangles represent 20 manually positioned adjacent regions of interest
485 (ROIs, 20 x 5 pixels). These ROIs are vertically aligned along the middle of the bolus, beginning at the
486 edge of bolus.
487

488
489 To quantify the changes over time and differences between the treatments grey value
490 changes across the bolus were examined (Figure 7A). The GLMM showed a main
491 effects of enzyme treatment ($\chi^2=69$, $p_{\text{FDR}}<0.0001$) and digestion time ($\chi^2=310$, p_{FDR}
492 <0.0001), as well as an interaction of treatment and time ($\chi^2=19.5$, $p_{\text{FDR}}=0.022$).



493 From 10 minutes onwards, the slope of the grey value curves for boli with amylase
 494 was consistently lower than that for pepsin-treated boli and boli with no enzyme
 495 (Table 3). The greatest difference between amylase-treated and pepsin treated boli
 496 was found at t=30 min. The slope of amylase-treated boli was 54% lower than that
 497 of pepsin-treated boli ($p < 0.0001$). At t=60 min, the slope of amylase-treated boli
 498 was 47% of that of no enzyme boli. There was no difference in slope between no-
 499 enzyme and pepsin-treated boli (all $p \geq 0.18$).



500 **Figure 7.** Mean±SD grey value of ROIs over 90 minutes digestion. (A) Example of a bolus ultrasound
 501 image with 20 adjacent ROIs. The first ROI at the edge of bolus is defined as 0 mm in the graphs, and
 502 last one is located at ~ 26 mm depth. Panels (B)-(F) show the mean grey value of the ROIs at 0, 10,
 503 30, 60 and 90 min, respectively, comparing among boli with amylase, pepsin and no enzymes. All
 504 measurements were done in triplicate.

505



506 **Table 3.** Pairwise comparisons for the Treatments × Time interaction on the slope of the grey value
507 curves.

Treatment Comparison	Time (min)	Ratio ¹	95% CI	p
Amylase / No enzyme	0	1.01	0.69, 1.48	0.996
	10	0.53	0.37, 0.78	<0.001
	30	0.53	0.31, 0.67	<0.001
	60	0.47	0.32, 0.69	<0.0001
	90	0.50	0.34, 0.73	<0.0001
Amylase / Pepsin	0	0.84	0.58, 1.23	0.53
	10	0.58	0.40, 0.84	0.002
	30	0.46	0.31, 0.67	<0.0001
	60	0.58	0.40, 0.84	0.002
	90	0.66	0.45, 0.97	0.028

508
509 ¹Estimated ratio of marginal mean slope of the grey value curves for amylase-treated boli to that of no
510 enzyme boli or the pepsin-treated boli. Ratio and 95% CI are back-transformed from GLMM contrasts
511 on the log scale.

512 The differences in slopes of grey value curves of ROIs with increasing depth may be
513 attributed to water absorption and associated physical changes during digestion. As
514 the SGF infiltrated and digestion progressed, the structure of amylase-treated boli
515 became looser, with the wrapped air pockets and porous bread structure being filled
516 by gastric fluid. This led to a more uniform internal texture which facilitated deeper
517 ultrasound transmission and more echo signal at internal interfaces. In contrast, the
518 no enzyme boli and the pepsin-treated boli did not expand rapidly and were not



519 visibly degraded. Overall, the looser structure, lower density, and rapidly dissolving
520 air in amylase-treated boli can lead to deeper sound wave penetration, resulting in a
521 slower decrease in grey value over imaging depth reflected by lower slope. These
522 results suggest that slope of grey value curves can be an indicator of changes in boli
523 properties during digestion, since it may reflect variations in signal intensity related
524 to sound wave transmission.

525 3.2 Changes in bolus moisture content and density

526 Both bolus mean grey value and the image texture features of amylase treated boli
527 differed from those of boli with pepsin and no enzyme. These differences are likely
528 related to structural and physical changes associated with the starch hydrolysis.

529 To further investigate the underlying causes, we compared the density and moisture
530 content of amylase boli before and after digestion (as shown in Figure S5 in
531 Supplementary data). Contrary to the possible interpretation mentioned above in
532 3.1.1, i.e., that variations in density will influence echogenicity, one-way ANOVA
533 result showed that there were no apparent changes in density over time ($p=0.55$).
534 However, it must be noted that echogenicity is related to density changes on a
535 microstructural level and not on a macro level. Furthermore, the lack of detectable
536 changes in density may be partially attributed to methodological factors. The density
537 of bread boli is close to that of water, and the drainage measurement used may be
538 insensitive to small variations. Moreover, as digestion progressed, the peripheral
539 regions of the boli tended to expand, where the density changed more significantly
540 than in the core. However, when the boli were removed from the digestive solution,
541 some water absorbed at the periphery was lost, so only the density of the denser



542 core, which retained a similar density as that of undigested boli, could be measured.

543 These factors may contribute to an overestimation of density.

544 Moisture content increased during digestion. A one-way ANOVA with time as the
545 independent factor and moisture as the dependent factor showed a main effect of
546 time ($F(4,10)=6.31$, $p=0.008$). Post-hoc Tukey tests showed that moisture at 10 min
547 ($\text{Mean}\pm\text{SD}=60.6\pm 3.09$, $p=0.062$) and 30 min ($\text{Mean}\pm\text{SD}=58.6\pm 1.61$, $p=0.21$) did
548 not differ from 0 min ($\text{Mean}\pm\text{SD}=52.8\pm 2.60$). Bolus moisture at 60 min
549 ($\text{Mean}\pm\text{SD}=62.5\pm 4.67$, $p=0.019$) and 90 min ($\text{Mean}\pm\text{SD}=64.1\pm 2.32$, $p=0.007$)
550 were higher than at 0 min. No other pairwise differences were found (all $p>0.24$).

551 The slight increase in moisture content may have contributed to deeper sound wave
552 penetration and reduced scattering. An *ex vivo* study investigated the use of
553 ultrasound to measure muscle dehydration, and found that when other tissue
554 components including proteins and fat remained constant, ultrasound velocity
555 increased with volumetric water loss.³¹ As acoustic impedance is the product of
556 density and sound speed, if bolus density remained stable or slightly decreased, and
557 the sound speed decreased because of higher water content, acoustic impedance
558 would decrease. This would allow sound waves to penetrate deeper and increase
559 reflection, which expands the detectable bolus area on ultrasound images. Therefore,
560 we speculate that the 5-10% increase in water content that we observed would be
561 sufficient to produce differences in sound wave amplitudes. However, similar to what
562 discussed for density measurements, moisture measurement may also have suffered
563 from methodological limitations. The swollen outer bolus layers may indeed affect
564 the accuracy of moisture measurements, because it is difficult to collect and measure
565 precisely how much water was incorporated into the boli. As the fluid penetrates from



566 the exterior to the interior, the periphery would have a higher water content than the
567 core, which was confirmed by the dry and porous structures in the core of the boli
568 even after 90 min digestion. However, when the boli were removed from the solution,
569 water retained in those fully water-filled bread chunks tended to be lost, leading to
570 an underestimation of water content. Examples are shown in Figure S6 in
571 Supplementary data.

572 3.3 Static *in vitro* starch and protein digestion in boli

573 Starch digestibility in the amylase treated boli increased progressively, from baseline
574 to 10 minutes and from 30 to 60 minutes, reaching approximately 22%, and ended
575 with a plateau (Figure S7 in Supplementary data). While it is well-known that amylase
576 becomes inactive at low pH, it can remain active for some time due to the buffering
577 capacity of food, until the pH gradually drops to around 3.5.³² Some studies show
578 that, before being inactivated by the acidic gastric environment, 30-80% of starch
579 can be hydrolysed, with up to half of it being broken down into oligosaccharides.^{33,34}

580 It should be noted that the degree of starch hydrolysis may be overestimated because
581 the GOPOD assay includes a step to convert starch-derived intermediates into glucose.
582 However, because this step was applied consistently across all time points, the trends
583 and comparisons among digestion intervals remain valid.

584 In contrast, protein hydrolysis, as reflected by the release of amino acid groups,
585 remained low throughout the whole digestion period and did not exceed 1%. This
586 limited extent of protein digestion may be attributed to the fact that the majority of
587 proteins in wheat flour are gluten proteins, which are mainly composed of gliadin and



588 glutenin. Their high proline and glutamine content contribute to their resistance to
589 gastric proteolysis.³⁵⁻³⁷

590 The digestion trends measured aligned with the ultrasound imaging results. The
591 greater degree of expansion and structural breakdown represented by the slopes was
592 correlated with the digestibility of starch ($\rho=-0.85$, $p_{\text{FDR}}<0.0001$) and protein
593 ($\rho=-0.76$, $p_{\text{FDR}}<0.01$) (Figure S8 in Supplementary data). In images of amylase-
594 treated boli, *homogeneity* showed a significant positive correlation with starch
595 digestibility ($\rho=0.8$, $p_{\text{FDR}}<0.0001$), while *entropy* showed a significant negative
596 correlation ($\rho=-0.81$, $p_{\text{FDR}}<0.0001$). In pepsin-treated boli, moderate correlations
597 were observed between protein hydrolysis and *homogeneity* ($\rho=0.52$, $p_{\text{FDR}}=0.048$)
598 and *entropy* ($\rho=-0.59$, $p_{\text{FDR}}=0.024$). These findings support the interpretation that
599 ultrasound image features can reflect structural degradation associated with starch
600 hydrolysis in bread boli. Although statistically significant correlations were found in
601 the pepsin treatment boli, the extremely low level of protein hydrolysis suggests that
602 visual expansion does not necessarily correspond to biochemical breakdown in
603 samples with low protein content. Bread was selected as a model food due to its
604 relatively uniform structure, however our ultrasound imaging approach is not
605 restricted to this substrate and may be used for a wide range of food matrices with
606 varying compositions and structural properties. A clearer relationship between
607 protein hydrolysis and image features may be observed in protein-rich foods.

608 A limitation of the present study relates to the segmentation of bolus regions on the
609 ultrasound images. Although the wand tool in QuPath applies consistent parameter
610 settings, the adjustment of the semi-automatic segmentation remains partly
611 operator-dependent. The seed selection sensitivity was assessed on representative



612 images, suggesting that seed selection had limited effect on area measurements and
613 on solidity as a measure of shape. In images with clear contrast between bolus and
614 background, segmentation was generally consistent. However, when the boundary
615 became less distinct, the delineation became less precise which may introduce minor
616 variability. This limitation is inherent to image-based ROI selection. Regarding the
617 degree of hydrolysis, a limitation is that amylase and pepsin were measured in
618 separate treatments rather than together. This was a practical compromise to
619 preserve analytical clarity. By isolating each enzyme's effect, the observed structural
620 and hydrolysis-related changes could be more directly attributed to a specific
621 enzymatic mechanism. Moreover, the large volume of SGF, constrained by technical
622 requirements associated with the pressure of the surrounding water and imaging
623 setup, resulted in a low bolus-to-fluid ratio. Dilution of hydrolysis products may
624 reduce detection sensitivity, particularly for protein digestion. Future work could
625 optimize the system to better mimic normal physiology. In addition, the digestion
626 chamber is compatible with MRI, which could further characterize bolus breakdown,
627 bolus internal structure and fluid distribution during digestion to inform the
628 interpretation of ultrasound measurements, representing a direction for future
629 research.

630 **4 Conclusion**

631 In conclusion, this study designed and applied an *in vitro* model compatible with
632 ultrasound imaging to investigate the structural breakdown of standardized bread
633 boli during gastric digestion. In addition to demonstrating that ultrasonography can
634 capture how enzymes affect the structural degradation during controlled gastric



635 digestion, grey value analysis and image texture metrics such as homogeneity and
636 entropy were used to characterize the imaged boli, showing their potential as non-
637 invasive indicators of digestibility and physical transformation. This proof-of-principle
638 study established a foundation for broader research on bolus breakdown of multiple
639 boli across different food matrices, and future work could extend these methods to
640 dynamic *in vitro* and *in vivo* digestion.

641 CRedit authorship contribution statement

642 **Xinhang Li:** Writing – original draft, Writing – review & editing, Conceptualization,
643 Methodology, Investigation, Formal analysis, Data curation, Visualization. **Edoardo**
644 **Capuano:** Writing – review & editing, Supervision, Project administration,
645 Conceptualization, Methodology, Validation, Resources. **Chris L. de Korte:** Writing
646 – review & editing, Supervision, Conceptualization, Methodology, Validation. **Paul**
647 **A.M. Smeets:** Writing – review & editing, Supervision, Project administration,
648 Conceptualization, Methodology, Validation, Resources.

649 Conflicts of interest

650 There are no conflicts to declare.

651 Data availability

652 The data supporting this article have been included as part of the supplementary.

653 Raw data can be made available upon request at corresponding author's email address.

654 Acknowledgements



655 The authors would like to thank Johan Belgraver of the AFSG Technical Development
656 Studio for building the *in vitro* setup, Iman Ibrahim for the first pilot testing and Dr. João
657 Caldas Paulo for her help during data analysis. We also gratefully acknowledge the input
658 of Eus Schrauwen (Vallei Medical, Ede, NL) and Eric de Groot, MD PhD (Imagelabonline
659 & Cardiovascular, Diepenheim, NL). X.L. acknowledges financial supported by the China
660 Scholarship Council (Grant No. 202309110023).

661



662 **References**

- 663 1. Bohn T, Carriere F, Day L, Deglaire A, Egger L, Freitas D, et al. Correlation between in vitro and in
664 vivo data on food digestion. What can we predict with static in vitro digestion models? *Crit Rev*
665 *Food Sci Nutr.* 2018;58(13):2239–61.
- 666 2. Shani-Levi C, Alvito P, Andrés A, Assunção R, Barberá R, Blanquet-Diot S, et al. Extending in vitro
667 digestion models to specific human populations: Perspectives, practical tools and bio-relevant
668 information. *Trends Food Sci Technol.* 2017;60:52–63.
- 669 3. Brodkorb A, Egger L, Alming M, Alvito P, Assunção R, Ballance S, et al. INFOGEST static in vitro
670 simulation of gastrointestinal food digestion. *Nat Protoc.* 2019;14(4):991–1014.
- 671 4. Tan Y, Zhou H, McClements DJ. Application of static in vitro digestion models for assessing the
672 bioaccessibility of hydrophobic bioactives: A review. *Trends Food Sci Technol* [Internet].
673 2022;122(February):314–27. Available from: <https://doi.org/10.1016/j.tifs.2022.02.028>
- 674 5. Smeets PAM, Deng R, Van Eijnatten EJM, Mayar M. Monitoring food digestion with magnetic
675 resonance techniques. *Proc Nutr Soc.* 2021 May 1;80(2):148–58.
- 676 6. Smith SW, Lopez H. A contrast-detail analysis of diagnostic ultrasound imaging. *Med Phys*
677 [Internet]. 1982 Jan 1;9(1):4–12. Available from: <https://doi.org/10.1118/1.595218>
- 678 7. Zhang G, Huang X, Shui Y, Luo C, Zhang L. Ultrasound to guide the individual medical decision by
679 evaluating the gastric contents and risk of aspiration: A literature review. *Asian J Surg.*
680 2020;43(12):1142–8.
- 681 8. Hlebowicz J, Jönsson JM, Lindstedt S, Björgell O, Darwich G, Almér LO. Effect of commercial rye
682 whole-meal bread on postprandial blood glucose and gastric emptying in healthy subjects. *Nutr J.*
683 2009;8(1):26.
- 684 9. Liu W, Jin W, Wilde PJ, Jin Y, Pan Y, Han J. Understanding the mechanism of high viscosity food
685 delaying gastric emptying. *Food Funct.* 2024;15(10):5382–96.
- 686 10. Sakata Y, Yago T, Mori S, Seto N, Matsunaga Y, Nakamura H, et al. Time Courses of Gastric
687 Volume and Content after Different Types of Casein Ingestion in Healthy Men: A Randomized
688 Crossover Study. *J Nutr* [Internet]. 2022;152(11):2367–75. Available from:
689 <https://doi.org/10.1093/jn/nxac158>
- 690 11. Giacomozzi AS, Benedito J, Quiles A, García-Pérez J V., Dalmau ME. Ultrasonic monitoring of
691 softening in solid foods during in-vitro gastric digestion. *J Food Eng.* 2024;374(January).
- 692 12. Avila-Sierra A, Decerle N, Ramaioli M, Peyron MA. Effect of salivary fluid characteristics on the
693 physical features of in vitro bread bolus: from the absence of saliva to artificially simulated
694 hypersalivation. *Food Res Int.* 2024;175:113753.
- 695 13. Gao J, Lin S, Jin X, Wang Y, Ying J, Dong Z, et al. In vitro digestion of bread: How is it influenced by
696 the bolus characteristics? *J Texture Stud.* 2019;50(3):257–68.
- 697 14. Bankhead P, Loughrey MB, Fernández JA, Dombrowski Y, McArt DG, Dunne PD, et al. QuPath:
698 Open source software for digital pathology image analysis. *Sci Rep.* 2017;7(1):1–7.
- 699 15. Haralick RM, Dinstein I, Shanmugam K. Textural Features for Image Classification. *IEEE Trans Syst*



- 700 Man Cybern. 1973;SMC-3(6):610–21.
- 701 16. Brynolfsson P, Nilsson D, Torheim T, Asklund T, Karlsson CT, Trygg J, et al. Haralick texture
702 features from apparent diffusion coefficient (ADC) MRI images depend on imaging and pre-
703 processing parameters. *Sci Rep* [Internet]. 2017;7(1):4041. Available from:
704 <https://doi.org/10.1038/s41598-017-04151-4>
- 705 17. Caruso D, Zerunian M, Ciolina M, de Santis D, Rengo M, Soomro MH, et al. Haralick's texture
706 features for the prediction of response to therapy in colorectal cancer: a preliminary study.
707 *Radiol Med*. 2018 Mar;123(3):161–7.
- 708 18. Mansour IR, Thomson RM. Haralick texture feature analysis for characterization of specific
709 energy and absorbed dose distributions across cellular to patient length scales. *Phys Med Biol*.
710 2023 Mar;68(7).
- 711 19. Wibmer A, Hricak H, Gondo T, Matsumoto K, Veeraraghavan H, Fehr D, et al. Haralick texture
712 analysis of prostate MRI: utility for differentiating non-cancerous prostate from prostate cancer
713 and differentiating prostate cancers with different Gleason scores. *Eur Radiol*. 2015
714 Oct;25(10):2840–50.
- 715 20. Schindelin J, Arganda-Carreras I, Frise E, Kaynig V, Longair M, Pietzsch T, et al. Fiji: An open-
716 source platform for biological-image analysis. *Nat Methods*. 2012;9(7):676–82.
- 717 21. Kong F, Singh RP. Modes of disintegration of solid foods in simulated gastric environment. *Food*
718 *Biophys*. 2009;4(3):180–90.
- 719 22. Freitas D, Gómez-Mascaraque LG, Brodkorb A. Digestion of protein and toxic gluten peptides in
720 wheat bread, pasta and cereal and the effect of a supplemental enzyme mix. *Front Nutr*.
721 2022;9:986272.
- 722 23. Byra M, Wan L, Wong JH, Du J, Shah SB, Andre MP, et al. Quantitative Ultrasound and B-Mode
723 Image Texture Features Correlate with Collagen and Myelin Content in Human Ulnar Nerve
724 Fascicles. *Ultrasound Med Biol*. 2019;45(7):1830–40.
- 725 24. van Eijnatten EJM, Camps G, Guerville M, Fogliano V, Hettinga K, Smeets PAM. Milk coagulation
726 and gastric emptying in women experiencing gastrointestinal symptoms after ingestion of cow's
727 milk. *Neurogastroenterol Motil*. 2023;(September):1–11.
- 728 25. Marciani L, Pritchard SE, Hellier-Woods C, Costigan C, Hoad CL, Gowland PA, et al. Delayed gastric
729 emptying and reduced postprandial small bowel water content of equicaloric whole meal bread
730 versus rice meals in healthy subjects: novel MRI insights. *Eur J Clin Nutr*. 2013 Jul;67(7):754–8.
- 731 26. Nadia J, Bronlund JE, Singh H, Singh RP, Bornhorst GM. Contribution of the proximal and distal
732 gastric phases to the breakdown of cooked starch-rich solid foods during static in vitro gastric
733 digestion. *Food Res Int* [Internet]. 2022;157:111270. Available from:
734 <https://www.sciencedirect.com/science/article/pii/S0963996922003271>
- 735 27. Mitrea D, Socaciu M, Badea R, Golea A. Texture based characterization and automatic diagnosis
736 of the abdominal tumors from ultrasound images using third order GLCM features. In: 2011 4th
737 International Congress on Image and Signal Processing. 2011. p. 1558–62.
- 738 28. Sultan LR, Venkatakrisna SSB, Anupindi SA, Andronikou S, Acord MR, Otero HJ, et al. ChatGPT-4–
739 Driven Liver Ultrasound Radiomics Analysis: Diagnostic Value and Drawbacks in a Comparative



- 740 Study. JMIR AI [Internet]. 2025;4:e68144. Available from: <https://ai.jmir.org/2025/1/e68144>
- 741 29. Guo R, Zhong H, Xing F, Lu F, Qu Z, Tong R, et al. Magnetic susceptibility and R2*-based texture
742 analysis for evaluating liver fibrosis in chronic liver disease. Eur J Radiol [Internet].
743 2023;169(August):111155. Available from: <https://doi.org/10.1016/j.ejrad.2023.111155>
- 744 30. van Eijnatten EJM, Camps G, Rombouts W, Pellis L, Smeets PAM. Gastric digestion and changes in
745 serum amino acid concentrations after consumption of casein from cow and goat milk: a
746 randomized crossover trial in healthy men. medRxiv [Internet]. 2024 Jan 1;2024.04.10.24305606.
747 Available from: <http://medrxiv.org/content/early/2024/04/24/2024.04.10.24305606.abstract>
- 748 31. Sarvazyan A, Tatarinov A, Sarvazyan N. Ultrasonic assessment of tissue hydration status.
749 Ultrasonics [Internet]. 2005;43(8):661–71. Available from:
750 <https://www.sciencedirect.com/science/article/pii/S0041624X05000120>
- 751 32. Rosenblum JL, Irwin CL, Alpers DH. Starch and glucose oligosaccharides protect salivary-type
752 amylase activity at acid pH. Am J Physiol - Gastrointest Liver Physiol. 1988;254(5).
- 753 33. Freitas D, Le Feunteun S. Oro-gastro-intestinal digestion of starch in white bread, wheat-based
754 and gluten-free pasta: Unveiling the contribution of human salivary α -amylase. Food Chem
755 [Internet]. 2019;274:566–73. Available from: <https://doi.org/10.1016/j.foodchem.2018.09.025>
- 756 34. Freitas D, Le Feunteun S, Panouillé M, Souchon I. The important role of salivary α -amylase in the
757 gastric digestion of wheat bread starch. Food Funct. 2018;9(1):200–8.
- 758 35. Stepniak D, Spaenij-Dekking L, Mitea C, Moester M, De Ru A, Baak-Pablo R, et al. Highly efficient
759 gluten degradation with a newly identified prolyl endoprotease: Implications for celiac disease.
760 Am J Physiol - Gastrointest Liver Physiol. 2006;291(4):621–9.
- 761 36. Cristofori F, Francavilla R, Capobianco D, Dargenio VN, Filardo S, Mastromarino P. Bacterial-Based
762 Strategies to Hydrolyze Gluten Peptides and Protect Intestinal Mucosa. Front Immunol.
763 2020;11(November).
- 764 37. Shewry PR, Halford NG. Cereal seed storage proteins: structures, properties and role in grain
765 utilization. J Exp Bot [Internet]. 2002 Apr 15;53(370):947–58. Available from:
766 <https://doi.org/10.1093/jexbot/53.370.947>

767



Data availability

View Article Online
DOI: 10.1039/D5FO04784F

The data supporting this article have been included as part of the supplementary.

Raw data can be made available upon request at corresponding author's email address.

